A Simplified Local Control Model of Calcium-Induced Calcium Release in Cardiac Ventricular Myocytes

R. Hinch,* J. L. Greenstein,† A. J. Tanskanen,† L. Xu,† and R. L. Winslow†
*Mathematical Institute, University of Oxford, Oxford, United Kingdom; and †The Center for Cardiovascular Bioinformatics and Modeling and The Whitaker Biomedical Engineering Institute, The Johns Hopkins University Whiting School of Engineering and School of Medicine, Baltimore, Maryland

ABSTRACT Calcium (Ca^{2+})-induced Ca^{2+} release (CICR) in cardiac myocytes exhibits high gain and is graded. These properties result from local control of Ca^{2+} release. Existing local control models of Ca^{2+} release in which interactions between L-Type Ca^{2+} channels (LCCs) and ryanodine-sensitive Ca^{2+} release channels (RyRs) are simulated stochastically are able to reconstruct these properties, but only at high computational cost. Here we present a general analytical approach for deriving simplified models of local control of CICR, consisting of low-dimensional systems of coupled ordinary differential equations, from these more complex local control models in which LCC-RyR interactions are simulated stochastically. The resulting model, referred to as the coupled LCC-RyR gating model, successfully reproduces a range of experimental data, including L-Type Ca^{2+} current in response to voltage-clamp stimuli, inactivation of LCC current with and without Ca^{2+} release from the sarcoplasmic reticulum, voltage-dependence of excitation-contraction coupling gain, graded release, and the force-frequency relationship. The model does so with low computational cost.

INTRODUCTION

The local-control theory of excitation-contraction (EC) coupling (Bers, 1993; Sham, 1997; Stern, 1992; Wier et al., 1994) asserts that opening of individual L-Type Ca^{2+} channels (LCCs) located in the *t*-tubule membrane triggers Ca^{2+} release from a small cluster of Ca^{2+} release channels, known as ryanodine receptors (RyRs), located in the closely apposed junctional sarcoplasmic reticulum (JSR) membrane. Tight regulation of Ca^{2+}-induced Ca^{2+}-release (CICR) is made possible by the fact that LCCs and RyRs are sensitive to the local concentration of Ca^{2+} within the dyadic space rather than global cytosolic Ca^{2+} levels. Graded control of JSR Ca^{2+} release, in which Ca^{2+}-release is a smooth, continuous function of LCC Ca^{2+} influx, is achieved by statistical recruitment of JSR Ca^{2+} release events (Beuckelmann and Wier, 1988; Stern, 1992; Wier and Balke, 1999).

Two classes of simplified EC coupling models have been developed and used in ventricular myocyte models. In the first, the Ca^{2+} release flux is represented as an explicit function of sarcolemmal Ca^{2+} influx (Faber and Rudy, 2000; Luo and Rudy, 1994). Models of this type can exhibit both high gain and graded SR Ca^{2+} release, but they lack mechanistic descriptions of the processes that are the underlying basis of CICR. In the second, known as *common pool models* (Stern, 1992), the flux of trigger Ca^{2+} through all LCCs as well as the Ca^{2+} release flux through all RyRs are each represented as single currents directed into a common Ca^{2+} pool (Jafri et al., 1998; Noble et al., 1998; Winslow et al., 1999). The result of this physical arrangement is that once RyR Ca^{2+} release is initiated, the resulting increase of Ca^{2+} concentration in the common pool stimulates regenerative, all-or-none rather than graded Ca^{2+} release (Stern, 1992). In addition to triggering SR Ca^{2+} release, increases of local Ca^{2+} promote Ca^{2+}-dependent inactivation of LCCs (Peterson et al., 1999). In existing computational models of the cardiac ventricular myocyte, inactivation of LCCs is dominated by voltage-dependent inactivation (Winslow et al., 2001). More recent data collected under conditions where Ca^{2+}-dependent inactivation of LCCs is selectively ablated (Alseikhan et al., 2002; Peterson et al., 1999) clearly demonstrate that relative to the timescale of the action potential (AP), Ca^{2+}-mediated inactivation of LCCs is rapid and strong, whereas voltage-dependent inactivation is slow and weak (Linz and Meyer, 1998; Peterson et al., 1999). When this relationship is incorporated into common pool models, AP duration becomes unstable—cycling between large and small values (Greenstein and Winslow, 2002), which renders such models useless for simulation of the AP. This loss of stability is a direct consequence of the all-or-none Ca^{2+} release property of common pool models, as it in turn produces all-or-none inactivation of inward LCC current during the plateau phase of the AP (Greenstein and Winslow, 2002).

We have recently formulated a computational model of the cardiac ventricular myocyte incorporating local control of CICR (Greenstein and Winslow, 2002). The model describes Ca^{2+} release units (CaRUs) consisting of a dyadic space in which individual sarcolemmal LCCs interact in a stochastic manner with nearby RyRs. CaRU dynamics are simulated stochastically within each time step over which the global system of ordinary differential equations describing

Submitted July 16, 2004, and accepted for publication September 21, 2004.
Address reprint requests to Dr. Robert Hinch, Oxford University, Mathematical Institute, 24–29 St. Giles, Oxford OX1 3LB UK. Tel.: 44-1-865-280-614; E-mail: hinch@maths.ox.ac.uk.

0006-3495/04/12/3723/14 $2.00
doi: 10.1529/biophysj.104.049973

membrane ionic and pump/exchanger currents, SR Ca^{2+} uptake, and time-varying cytosolic ion concentrations are solved. The model incorporates the experimentally observed strong negative feedback coupling between RyR Ca^{2+} release and LCC current. The model accurately reconstructs stable APs and describes critical features of CICR including graded release and voltage-dependent gain. These results demonstrate that to accommodate new data regarding strong negative feedback regulation of LCC function by JSR Ca^{2+} release, myocyte models must incorporate graded CICR. Unfortunately, local control models based on stochastic simulation of CaRU dynamics are far too computationally demanding to be used routinely in single cell simulations, let alone in models of cardiac tissue.

In this article, we formulate a novel model of CICR which describes the underlying channels and local control of Ca^{2+} release, but consists of a low dimensional system of ordinary differential equations. This is achieved in two steps, using the same techniques as applied by Hinch (2004) in an analysis of the generation of spontaneous sparks in a model of a cluster of RyRs. First, the underlying channel and CaRU models are minimal, such that they only contain descriptions of the essential biophysical features observed in EC coupling. This in turn yields a system of model equations which can be simplified by applying approximations based on a separation of timescales. In particular, it can be shown that $[Ca^{2+}]$ in the dyadic space (denoted $[Ca^{2+}]_{ds}$) equilibrates rapidly relative to the gating dynamics of the LCCs and RyRs. The joint behavior of LCCs and RyRs can then be described using a Markov model where the transition probabilities between interacting states are a function of global variables only. This in turn allows the ensemble behavior of the CaRUs to be calculated using ordinary differential equations. The resulting model, which we refer to as the coupled LCC-RyR gating model, has parameters which may be calculated directly from the underlying biophysical model of local control of Ca^{2+} release (see Table 1; for additional information, see Tables 2–4). We show that despite the simplicity of this model, it captures key properties of CICR including graded release and voltage-dependence of EC coupling gain. The great advantage of this novel approach is its increased computational efficiency. Simulations using the model presented in this article require up to 10^5 times less computation time and 10^5 less memory compared with previous local control models, which were also based on the underlying channel kinetics (Greenstein and Winslow, 2002). The model is therefore well suited for incorporation within single cell and tissue models of ventricular myocardium.

DERIVATION OF MODEL

Our aim is to formulate a computationally tractable model which sufficiently describes the underlying physiological mechanisms of EC coupling. To do this, we first develop a simple model of CaRUs consisting of continuous-time Markov chain descriptions of LCC and RyR gating. This model is then simplified by taking advantage of large separations of timescales. The resulting formulation consists of six coupled ordinary differential equations for the entire Ca^{2+} regulation system. The method described below is a general technique and can be applied to CICR models of any species. As an example, the model is calibrated using data acquired from experiments in rat.

TABLE 1 LCC and RyR parameters

Parameter	Definition	Value
V_L	Potential when half LCC open	-2 mV
ΔV_L	Width of opening potentials	7 mV
ϕ_L	Proportion of time closed in open mode	2.35
t_L	Time switching between C and O states	quick
τ_L	Inactivation time	650 ms
K_L	Concentration at inactivation	0.22 μM
a	Biasing to make inactivation function of V	0.0625
b	Biasing to make inactivation function of V	14
J_L	Permeability of single LCC	9.13×10^{-4} $\mu m^3\ ms^{-1}$
K_{RyR}	Half concentration of activation	41 μM
t_R	Time switching between C and O states	1.17 t_L
ϕ_R	Proportion of time closed in open mode	0.05
τ_R	Inactivation time	2.43 ms
θ_R	Reciprocal of proportion of time inactivated in open mode	0.012
c	Biasing to make inactivation a function of $[Ca^{2+}]_{ds}$	0.01
d	Biasing to make inactivation a function of $[Ca^{2+}]_{ds}$	100
J_R	Permeability of single RyR	2×10^{-2} $\mu m^3\ ms^{-1}$

To avoid confusion, when parameters from other models are referred to they are given a tilde. V_L and ΔV_L are estimated by fitting the I-V curve for the LCC (Fig. 5). The LCC parameters $\phi_L = \tilde{g}/\tilde{f}$, $\tau_L = \tilde{b}^4/\tilde{\omega}$, $K_L = \tilde{\omega}/\tilde{b}^4\tilde{a}^4\tilde{\gamma}_0$, $a = 1/\tilde{a}^4$, $b = \tilde{b}^4$, and J_L are all from Greenstein and Winslow (2002). The RyR parameters $\phi_R = \tilde{k}_{O1C1}/\tilde{k}_{C1O1}$, and $t_R = 1/\tilde{k}_{O1C1}$ are from Zahradnikova and Zaradnik (1996); and $K_{RyR} = \sqrt{\tilde{K}_{OM}/\tilde{K}_O}$, $\tau_R = \phi_R/K_{RyR}\tilde{K}_I$, and $\theta_R = \tilde{K}_{IM}\tau_R$ are from Stern et al. (1999). (Note the parameter values for Scheme 6 were not given, so we estimated them from Scheme 5 in Stern et al., 1999.) The designations of c and d are chosen such that 1% of RyRs are inactivated at low $[Ca^{2+}]$, and J_R was chosen to fit the EC gain curve (Fig. 8 *B*).

The L-type Ca^{2+} channel (LCC) model

At low membrane potentials (<-40 mV) LCC open probability is essentially zero. Upon membrane depolarization, LCCs open and close stochastically with a mean open time of ~0.5 ms and a peak open probability of 5–15% (Rose et al., 1992; Herzig et al., 1993; Handrock et al., 1998). The primary mechanism of LCC inactivation is via Ca^{2+} binding to calmodulin which is tethered to the channel on the intracellular side. LCCs also undergo voltage-dependent inactivation; however, when considered over a timescale of the AP, this inactivation is far slower and less

TABLE 2 Physical constants and geometry

Parameter	Definition	Value
F	Faraday constant	96.5 C mmol^{-1}
T	Temperature	295 K
R	Universal gas constant	8.314 J mol^{-1} K^{-1}
V_{cyto}	Cytosolic volume	2.584×10^4 μm^3
V_{ds}	Volume of a single dyadic space	2.0×10^{-4} μm^3
V_{SR}	Volume of sarcoplasmic reticulum	2.098×10^3 μm^3
N	Number of release units	50,000
C_{AM}	Total membrane capacitance	1.534×10^{-4} μF

All values are from Bonderenko et al. (2004) except V_{ds} and N, which are from Greenstein and Winslow (2002). (Note that there are four LCCs per CaRU.)

complete than that produced by Ca^{2+} inactivation (Linz and Meyer, 1998; Peterson et al., 1999, 2000). The process of voltage-dependent inactivation is therefore ignored in this model.

Several detailed models of LCC gating have been formulated (Jafri et al., 1998; Bondarenko et al., 2004). We use a model which is a simplified version of the Jafri et al. (1998) model (Fig. 1 *A*). First, the state O_{Ca} is dropped from the 12-state model because its occupancy rate is nearly zero. Second, states C_0, C_1, C_2, and C_3, and I_0, I_1, I_2, and I_3, are combined to make a five-state Markov model (Fig. 1 *B*). The effect of this change is a minor alteration to the activation kinetics of the LCC, although the principle biophysical mechanisms (e.g., mode-switching, voltage-dependent activation, and Ca^{2+}-dependent inactivation) are retained. The five-state model consists of two closed states (denoted C_1 and C_2), a single open state O accessible from closed state C_2, and two Ca^{2+}-inactivated states I_1 and I_2 accessible from states C_1 and C_2, respectively. Transition rates into the inactivated states are a function of $[Ca^{2+}]_{ds}$. This model can be simplified to a three-state model (Fig. 1 *C*) by assuming that transitions between the state pairs C_1 and C_2, and I_1 and I_2, are rapid relative to the transition rates between these two

TABLE 3 Fixed ionic concentrations and buffers

Parameter	Definition	Value
$[Na^+]_e$	Extracellular $[Na^+]$	140 mM
$[Na^+]_i$	Intracellular $[Na^+]$	10 mM
$[Ca^{2+}]_e$	Extracellular $[Ca^+]$	1000 μM
$[B]_{CMDN}$	Total cytosolic calmodulin concentration	50.0 μM
K_{CMDN}	Half saturation constant of calmodulin	2.38 μM
$[B]_{TRPN}$	Total cytosolic troponin concentration	70.0 μM
k^+_{TRPN}	Binding rate of $[Ca^{2+}]$ to troponin	0.04 μM^{-1} ms^{-1}
k^-_{TRPN}	Disassociation rate of $[Ca^{2+}]$ to troponin	0.04 ms^{-1}
V_0	Resting potential	−80 mV
$[Ca^{2+}]_{i,0}$	Cytoplasmic $[Ca^{2+}]$ at V_0	0.1 μM
$[Ca^{2+}]_{SR,0}$	SR $[Ca^{2+}]$ at V_0	700 μM

Extracellular and intracellular concentrations $[Na^+]_e$, $[Na^+]_i$, $[Ca^{2+}]_e$, and $[Ca^{2+}]_{i,0}$ are from Stern et al. (1999); buffer concentrations $[B]_{CMDN}$ and K_{CMDN}, and resting $[Ca^{2+}]_{SR,0}$ are from Greenstein and Winslow (2002); and troponin parameters $[B]_{TRPN}$, k^+_{TRPN}, and k^-_{TRPN} are from Bonderenko et al. (2004).

TABLE 4 Other Ca^{2+} currents

Parameter	Definition	Value
g_D	Ca^{2+} flux rate from dyadic space to cytosol	0.065 μm^3 ms^{-1}
g_{SERCA}	Maximum pump rate of SERCA	0.45 μM ms^{-1}
K_{SERCA}	Half saturation of SERCA	0.5 μM
$r_{SR,l}$	Rate of leak from the SR to cytosol	1.9×10^{-5} ms^{-1}
K_{mNa}	Na^+ half saturation of NCX	87.5 mM
K_{mCa}	Ca^{2+} half saturation of NCX	1380 μM
η	Voltage dependence of NCX control	0.35
k_{sat}	Low potential saturation factor of NCX	0.1
g_{NCX}	Pump rate of NCX	38.5 μM ms^{-1}
g_{pCa}	Maximum pump rate of sarcolemmal pump	0.0035 μM ms^{-1}
K_{pCa}	Half saturation of sarcolemmal	0.5 μM
g_{Cab}	Conductance of background Ca^{2+} current	2.42×10^{-5} μM mV^{-1} ms^{-1}

The sarcolemmal channel parameters K_{mNa}, K_{mCa}, η, k_{sat}, and K_{pCa} are taken from Luo and Rudy (1994). The SERCA parameters K_{SERCA} and g_{SERCA} are from Bondarenko et al. (2004). The dyadic space conductance g_D is chosen to give $\tau_{ds} = 3$ μs (average of Sobie et al., 2002, and Greenstein and Winslow, 2002). The designations g_{NCX} and g_{pCa} are chosen to balance transmembrane flux of Ca^{2+} over each cycle. The leak conductances $r_{SR,l}$ and g_{Cab} are calculated to satisfy $[Ca^{2+}]_{i,0}$ and $[Ca^{2+}]_{SR,0}$.

sets of states. The transition rate from state C_4 to C_3 is rapid compared with the transition rate to state I_4. The rate from state C_4 to C_3 is approximately twice that of the transition rate to state O. Since the ratio of these two rates is not sufficiently large (i.e., >10), the reduced three-state model will exhibit slightly different activation kinetics than the five-state model. This discrepancy is not an issue since further model reductions (described below) will be based on the assumption of instantaneous LCC activation. Define the combined closed state $C = C_1 \cup C_2$ and the combined inactivated state $I = I_1 \cup I_2$. Since the timescale of the transitions between C_1 and C_2 is the smallest timescale in the model, we can assume that these two states are in equilibrium and thus define conditional state occupancy probabilities as

$$P(C_1|C) = \frac{\alpha_{-1}}{\alpha_1 + \alpha_{-1}} \quad \text{and} \quad P(C_2|C) = \frac{\alpha_1}{\alpha_1 + \alpha_{-1}}. \qquad (1)$$

A similar approximation is applied to states I_1 and I_2. Under these assumptions, the forward transition rate between the combined closed state C and the combined inactivated state I (Fig. 1 *B*) is given by

$$\epsilon_+([Ca^{2+}]_{ds}) = a\epsilon_1([Ca^{2+}]_{ds})P(C_1|C) + \epsilon_1([Ca^{2+}]_{ds})P(C_2|C). \qquad (2)$$

A similar approach may be used to derive the remaining transition rates among states I, C, and O (see Eq. 12). The open channel current is given by the Goldman-Hodgkin-Katz equation (see Eq. 13), where $[Ca^{2+}]$ at the intracellular mouth of the LCC is assumed to be equal to $[Ca^{2+}]_{ds}$. This model of the LCC is validated using voltage-clamp data

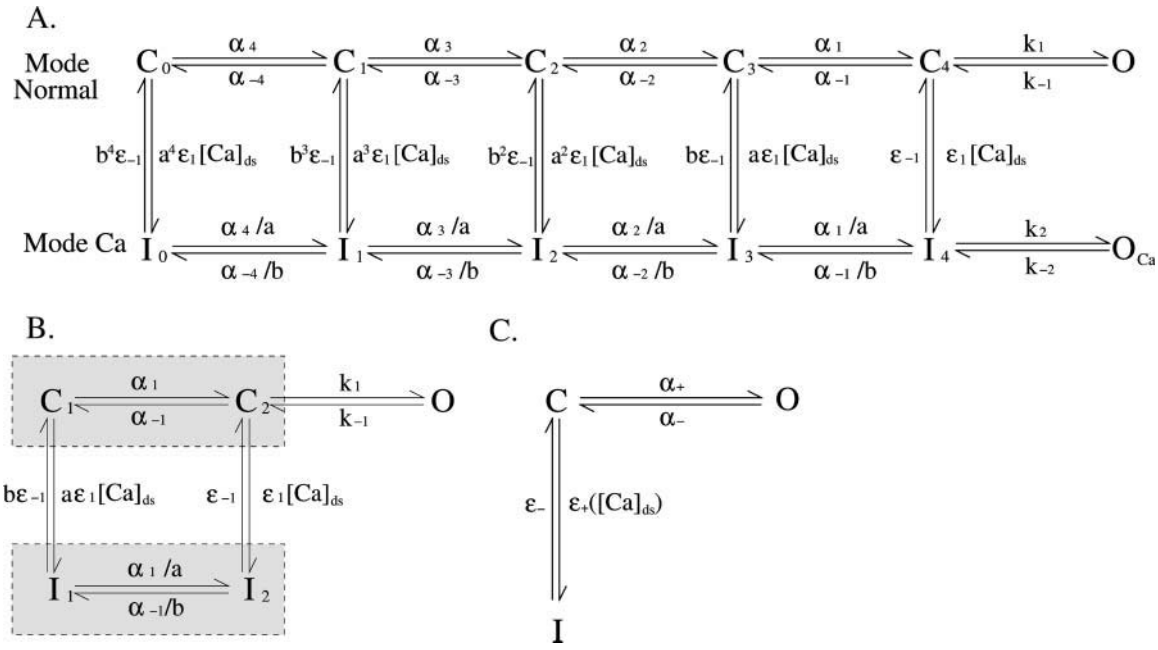

FIGURE 1 (*A*) The original 12-state model of the LCC (Jafri et al., 1998). (*B*) The five-state model of the LCC containing voltage-dependent activation, Ca^{2+}-dependent inactivation, and modal gating. The closed states C_1 and C_2 are grouped together to form a single state C, and the states I_1 and I_2 are grouped together to form a single state I. (*C*) The reduced three-state model of the LCC.

(Zahradnikova et al., 2004) in the following section (see Figs. 5 and 6).

The ryanodine receptor (RyR) model

When $[Ca^{2+}]_{ds}$ is near diastolic levels, the open probability of RyRs is small. When $[Ca^{2+}]_{ds}$ is increased, RyRs open and close stochastically on a timescale of ~2 ms (Zahradnikova and Zahradnik, 1995, 1996). In experiments on single RyRs in lipid bilayers where transient increases in Ca^{2+} are generated by flash photolysis, it has been demonstrated that the rate of activation of RyRs is sufficiently rapid (0.07–0.27 ms) to be triggered by single LCC openings (Zahradnikova et al., 1999). The Hill coefficient of activation with $[Ca^{2+}]_{ds}$ has been reported as ~2.5 (Zahradnikova et al., 1999). Experiments on single RyRs in lipid bilayers suggest that the time constant of inactivation is too slow (Zahradnikova and Zahradnik, 1996) to be important, even in the presence of physiological concentration of Mg^{2+} (Valdivia et al., 1995; Xu et al., 1996). However, experiments on whole cells suggest that RyR inactivation is the primary mechanism of termination of SR release (Sham et al., 1998). Whether RyRs contain a sufficiently rapid inactivation mechanism to be considered the primary process influencing the termination of SR Ca^{2+} release during EC coupling is still an open question (Stern and Cheng, 2004). Following the experiments of Sham et al. (1998) and previous models (e.g., Stern et al., 1999), our model contains RyR inactivation as the primary mechanism of termination of SR release.

We use a five-state model of the RyR (Fig. 2 *A*) based on Scheme 6 of Stern et al. (1999), with the addition of modal gating between the C and O states. (Note that Stern et al., 1999, presented six different schemes for the kinetics of the RyR, although only Schemes 5 and 6 could successfully model CICR.) Transitions from the closed to open modes occur upon binding of two Ca^{2+} ions. Transitions between states C_1 and C_2, and inactivated states I_1 and I_2, are assumed to be rapid. Following the same procedure used in the reduction of the LCC model, the RyR model is reduced to a three-state model (Fig. 2 *B*, see Eq. 14). The magnitude of the Ca^{2+} flux through an open RyR is proportional to the difference in $[Ca^{2+}]$ between the SR and the local dyadic space.

The calcium release unit (CaRU) model

We employ a minimal model for each CaRU (Fig. 3) consisting of one LCC, a closely apposed RyR, and the dyadic space within which these channels reside. Experimental recordings of triggered Ca^{2+}-sparks show that a single LCC opening may activate 4–6 RyRs (Wang et al., 2001). The CaRU model employed here is therefore a simplification of actual dyadic structure and function (see Discussion). Several models of CaRUs (e.g., Sobie et al., 2002; Greenstein and Winslow, 2002) also include a local junctional SR volume which is depleted relative to the network SR during Ca^{2+} release. However, recent experimental studies suggest that the junctional SR $[Ca^{2+}]$ is in quasi-equilibrium with network SR during Ca^{2+} release (Shannon et al., 2003). Therefore, the

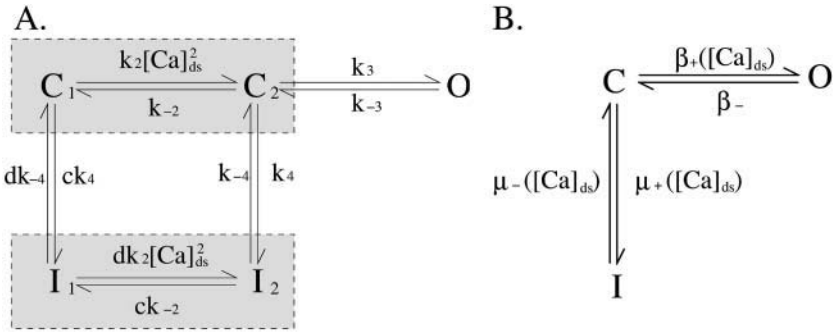

FIGURE 2 (*A*) The five-state model of the RyR containing Ca^{2+}-dependent activation, time-dependent inactivation, and modal gating. The closed states C_1 and C_2 are grouped together to form a single state C, and the states I_1 and I_2 are grouped together to form a single state I. (*B*) The reduced three-state model of the RyR.

minimal CaRU model does not include a local JSR compartment (see Discussion). The Ca^{2+} flux from the dyadic space to the myoplasm is governed by simple diffusion, such that the time-evolution of $[Ca^{2+}]_{ds}$ is given by

$$V_{ds}\frac{d[Ca^{2+}]_{ds}}{dt} = J_{RyR} + J_{LCC} - g_D([Ca^{2+}]_{ds} - [Ca^{2+}]_i), \quad (3)$$

where V_{ds} is the volume of the dyadic space, $[Ca^{2+}]_i$ is the $[Ca^{2+}]$ in the myoplasm, g_D is the Ca^{2+} flux rate between the dyadic space and bulk myoplasm, and J_{RyR} and J_{LCC} are the currents through the RyR and LCC, respectively. The time constant of equilibrium of $[Ca^{2+}]_{ds}$ is given by $\tau_{ds} = V_{ds}/g_D \approx 3\ \mu s$ (Sobie et al., 2002; Hinch, 2004). Since this time constant is considerably smaller than that for opening of either LCC or RyR channels, we may use the rapid equilibrium approximation (Hinch, 2004) to show that

$$[Ca^{2+}]_{ds} \sim [Ca^{2+}]_i + \frac{J_{RyR} + J_{LCC}}{g_D}. \quad (4)$$

This is the crucial step in model simplification since $[Ca^{2+}]_{ds}$ is now a function of only the global variables $[Ca^{2+}]_{SR}$, $[Ca^{2+}]_i$, V, and the state of the local RyR and LCC. As a result of this simplification, it is no longer necessary to solve a differential equation for each $[Ca^{2+}]_{ds}$ when modeling all CaRUs in the myocyte (this is the reason why previous local control models, such as Greenstein and Winslow, 2002, have been so computationally demanding). This approach has some similarities with the theory of Ca^{2+}-synapses (Stern, 1992; see Discussion).

Define y_{ij} (where $i, j = C, O, I$) as the state of the CaRU with the LCC in the i^{th} state and the RyR in the j^{th} state. The CaRU can then be in one of nine macroscopic states (Fig. 4 *A*). $[Ca^{2+}]_{ds}$, J_{RyR}, and J_{LCC} must be calculated separately for each of the nine states. For example, consider the state y_{CO} with the LCC closed ($J_{LCC} = 0$) and the RyR open ($J_{RyR} = J_R([Ca^{2+}]_{SR} - [Ca^{2+}]_{ds})$), then the rapid equilibrium approximation (Eq. 4) yields

$$\begin{aligned} c_{CO} &= \frac{[Ca^{2+}]_i + \dfrac{J_R}{g_D}[Ca^{2+}]_{SR}}{1 + \dfrac{J_R}{g_D}}, \\ J_{R,CO} &= J_R\frac{[Ca^{2+}]_{SR} - [Ca^{2+}]_i}{1 + \dfrac{J_R}{g_D}}, \end{aligned} \quad (5)$$

where c_{CO} is $[Ca^{2+}]_{ds}$ in the state y_{CO} and $J_{R,CO}$ is J_{RyR} in the state y_{CO}. Results for other states are listed in the Appendix Eqs. 16–19. The nine-state model of the CaRU is shown in Fig. 4 *A*. This model is what we refer to as the coupled LCC-

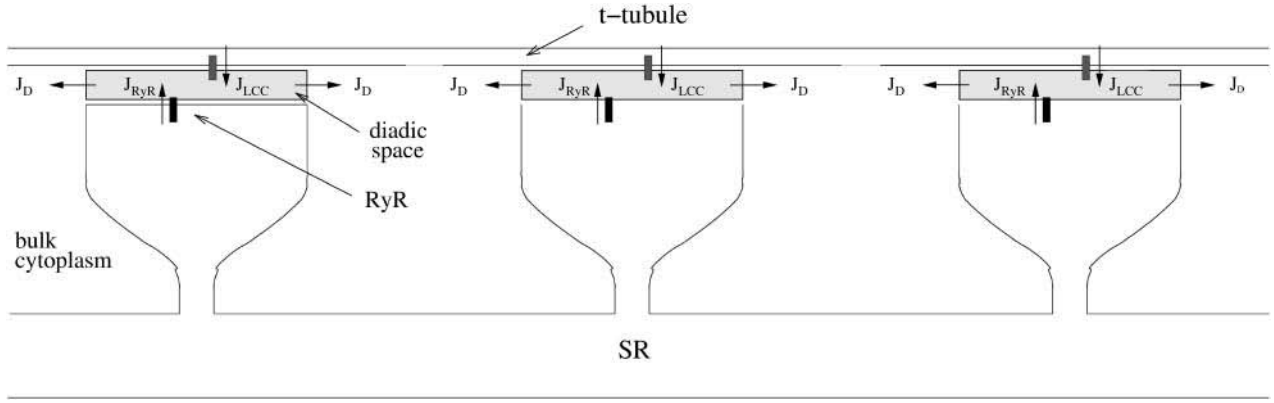

FIGURE 3 The geometry of the CaRU model. Although this diagram contains only three CaRUs, the overall model contains a large number of identical CaRUs. Each CaRU consists of a single LCC on a *t*-tubule and a single RyR on the SR facing into a dyadic space.

RyR gating model. Note that transitions are a function of $[Ca^{2+}]_{ds}$, which is itself a function of model states.

This model can be simplified further by taking advantage of the fact the mean open times of the RyR and LCC ($\approx$1 ms) are substantially shorter than the inactivation times ($\approx$20 ms) of either the LCC or RyR. The rapid equilibrium approximation is applied once again to simplify the model to a four-state model. Define the combined states $z_1 = y_{CC} \cup y_{CO} \cup y_{OC} \cup y_{OO}$, $z_2 = y_{OI} \cup y_{CI}$, $z_3 = y_{IC} \cup y_{IO}$, and $z_4 = y_{II}$. The rapid equilibrium approximation requires that the substates assume steady-state values; for example,

$$P(y_{OC}|z_1) = \frac{\alpha_+\beta_-(\alpha_+ + \alpha_- + \beta_- + \beta_+(c_{CC}))}{(\alpha_+ + \alpha_-)((\alpha_- + \beta_- + \beta_+(c_{OC}))(\beta_- + \beta_+(c_{CC})) + \alpha_+(\beta_- + \beta_+(c_{OC})))}. \quad (6)$$

Expressions for the other combined states are given in Eq. 20. Transition rates between combined states (Fig. 4 *B*) are found by summing the transitions from the substates; for example

$$r_1 = P(y_{OC}|z_1)\mu_+(c_{OC}) + P(y_{CC}|z_1)\mu_+(c_{CC}) \quad (7)$$

(see also Eq. 21). Finally, we use the law of mass action to derive differential equations for the evolution of the subpopulations of the CaRU (Eq. 22). The whole-cell Ca^{2+} currents are calculated by summing the contributions from all the populations of the CaRU where the relevant channel is open, as

$$I_{LCC} = \frac{N}{V_{cyto}}(J_{L,OO}P(y_{OO}|z_1) + J_{L,CO}P(y_{CO}|z_1))z_1 + \frac{N}{V_{cyto}}P(y_{OI}|z_2)z_2, \quad (8)$$

where N is the total number of CaRUs in the model and V_{cyto} is the volume of the cytoplasm. Note that the size of the current is different in each subpopulation. A similar expression for the RyR current is found in Eq. 23.

Whole-cell Ca^{2+} regulation

The CaRU model can now be incorporated within a standard model of whole-cell Ca^{2+} regulation. The total Ca^{2+} current directed into the bulk myoplasm is

$$I_i = I_{LCC} + I_{RyR} - I_{SERCA} + I_{SR,l} + I_{NCX} - I_{pCa} + I_{Cab} + I_{TRPN}. \quad (9)$$

The mathematical formulae for these currents are given in Eqs. 24–28. Ca^{2+} is resequestered into the SR via the SERCA pump (I_{SERCA}). $I_{SR,l}$ is a leak current from the SR to the bulk myoplasm and its conductance is chosen such that $[Ca^{2+}]_{SR} = 700\ \mu M$ when the cell is in equilibrium and voltage-clamped at -80 mV. The principle mechanism for Ca^{2+} removal from the cell is the sodium-calcium exchanger (I_{NCX}). A secondary transporter which removes Ca^{2+} from the cell is the sarcolemmal Ca^{2+}-ATPase (I_{pCa}). In rat myocytes, it has been estimated that the Ca^{2+}-ATPase contributes 24% of the Ca^{2+} removal during a Ca^{2+} transient (Sook Choi and Eisner, 1999). The final current is the background leak current (I_{Cab}) and its conductance is chosen so that $[Ca^{2+}]_i = 0.1\ \mu M$ when the cell is in equilibrium and voltage-clamped at -80 mV. Ca^{2+} is buffered by calmodulin and troponin (I_{TRPN}) in the bulk myoplasm. Buffering by calmodulin is rapid compared with the evolution of the $[Ca^{2+}]$, so the effect of the buffer can be modeled using the rapid buffer approximation (Wagner and Keizer, 1994). The rate of change of $[Ca^{2+}]$ is given by

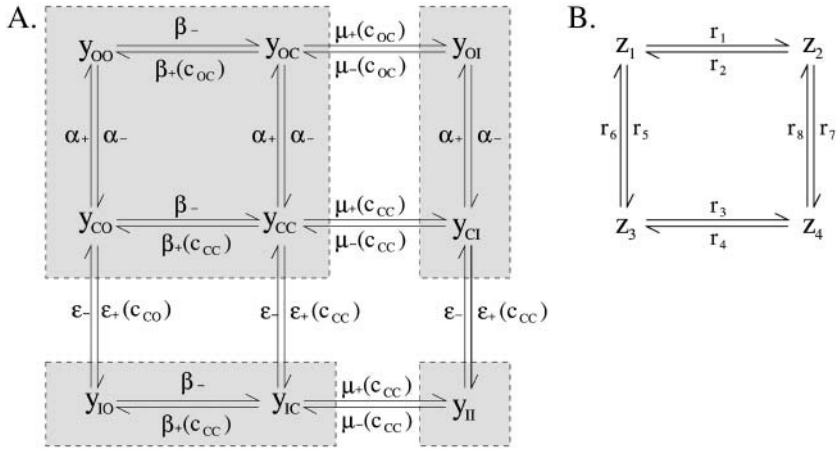

FIGURE 4 (*A*) The nine-state model of the CaRU. In state y_{ij}, the LCC is in the state i and the RyR is in the state j. Note that the transitions are a function of $[Ca^{2+}]_{ds}$ which is a function of state. (*B*) The simplified four-state model of the CaRU, after applying the approximation that open times are rapid.

$$\frac{d[Ca^{2+}]_i}{dt} = \beta_i I_i, \tag{10}$$

where I_i is given by Eq. 9,

$$\beta_i = \left(1 + \frac{K_{CMDN}[B]_{CMDN}}{(K_{CMDN} + [Ca^{2+}]_i)^2}\right)^{-1}, \tag{11}$$

and $[B]_{CMDN}$ and K_{CMDN} are the total concentration and half-saturation concentration of calmodulin, respectively. The full equations for the evolution of $[Ca^{2+}]$ in the bulk myoplasm and SR are given in Eq. 32.

RESULTS

Model properties are now compared with a range of experimental data chosen to test different aspects of Ca^{2+} regulation. These experimental results were used to determine the channel densities in the model. The equations were solved using a variable-step fourth-order Runge-Kutta integration algorithm (Press et al., 1989) on a PC with a 2-GHz processor and 512 Mb of RAM.

L-Type Ca^{2+} current

Two essential features of the L-type Ca^{2+} current are the peak I-V curve and inactivation dynamics. In particular, inactivation of LCCs is highly dependent upon properties of CICR. The ability to reproduce inactivation responses thus represents a good test of local control models (Zahradnikova et al., 2004). Fig. 5 *A* shows LCC current generated by a voltage step from −50 mV to a range of potentials between 0 mV and 30 mV. Fig. 5 *B* compares the model LCC peak I-V curve with that measured experimentally (Zahradnikova et al., 2004). Peak LCC current is defined as that in response to the indicated test potential (abscissa) from a holding potential of −50 mV. Model and experimental I-V curves are in close agreement. In voltage-clamp experiments in which SR Ca^{2+} is intact, it is found that the L-Type Ca^{2+} current is inactivated after ~20 ms. However, when SR Ca^{2+} is depleted by application of caffeine (Zahradnik and Palade, 1993), ryanodine (Balke and Wier, 1991), or application of prepulses (Delgado et al., 1999), Ca^{2+} inactivation is much slower (Sipido et al., 1995; Zahradnikova et al., 2004). Fig. 6, *A* and *B*, shows a comparison of the model prediction of this effect with experimental results (Zahradnikova et al., 2004). In both model and experiment, the cell was clamped at −50 mV and then stepped to 10 mV for 70 ms. The SR Ca^{2+} was depleted in the model by setting it to 10% of its normal value. The experimental and model results are in close agreement. Fig. 6, *C* and *D*, shows a comparison of the model and experiment for voltage steps from −50 mV to +10 mV, +20 mV, and +30 mV. The model successfully predicts the slower inactivation with steps to +30 mV compared with steps to +10 mV; however, since activation of the LCC current is assumed to be instantaneous in the model, the voltage-dependent changes in the activation kinetics are not captured by the model.

CICR and gain

Fig. 7 shows the intracellular $[Ca^{2+}]$ and the SR Ca^{2+} content in response to a voltage step from −80 mV to 0 mV for 200 ms with a basic cycle length of 400 ms. During the Ca^{2+} transient 40% of the SR Ca^{2+} is released, which is similar to experimental values (≈35%, Bassani et al., 1995; DelBridge et al., 1996). Fig. 8 *A* shows that the coupled LCC-RyR gating model captures the fundamental property of graded Ca^{2+} release, in that RyR current is a smooth, continuous function of trigger Ca^{2+}. In addition, it is now well established that Ca^{2+} release is most effective at those membrane potentials producing large single LCC currents (Wier et al., 1994). This results in the peak of I_{RyR} being shifted by ~10 mV in the hyperpolarizing direction relative to the peak of I_{LCC} . This important behavior is also captured by the coupled LCC-RyR gating model (Fig. 8 *A*). As a consequence of this relative displacement of peak values, EC coupling gain decreases with increasing membrane potential. Following Wier et al. (1994), we define the gain as the ratio of maximum of I_{RyR} with the maximum of I_{LCC} . Fig. 8 *B* shows that EC coupling gain predicted by the model is in agreement with experimental measurements (Wier et al., 1994; Cannell et al., 1995; Janczewski et al., 1995; Santana et al., 1996).

The final set of experiments examines the behavior of Ca^{2+} as a function of pacing frequency. The response of the Ca^{2+} regulation system to pacing frequency is nontrivial and is species-dependent (reviewed by Carmeliet, 2004). Human, rabbit, and guinea pig ventricular myocytes exhibit a positive force-frequency relationship, where the force of contraction increases with frequency (Carmeliet, 2004; Pieske et al., 1999; Maier et al., 2000), although in some experiments a dome-shaped force-frequency relationship has been observed (Boyett and Jewell, 1980). In rats both negative (Hoffman and Kelly, 1959; Maier et al., 2000) and positive (Frampton et al., 1991; Layland and Kentish, 1999) force-frequency relationships have been reported. The effect of frequency on the Ca^{2+} transient can be tested in the model. The model was excited periodically by a 200-ms-long step depolarization from −80 mV to 0 mV. Fig. 9 *A* shows the peak systolic $[Ca^{2+}]$, diastolic $[Ca^{2+}]$, and amplitude (defined as the peak systolic minus the diastolic) of the Ca^{2+} transient as a function of frequency for the model. Note that the systolic $[Ca^{2+}]$, diastolic $[Ca^{2+}]$, and amplitude of the Ca^{2+} transient all increase with frequency. Fig. 9 *B* shows experimental recordings of Ca^{2+} transients of paced rat ventricular trabeculae over the same range of frequencies (replotted from Fig. 2 *C* of Layland and Kentish, 1999). The intracellular $[Ca^{2+}]$ was measured using a Ca^{2+}-sensitive fluorescent dye. The experimental and model results exhibit a similar force-frequency relationship. The force-frequency

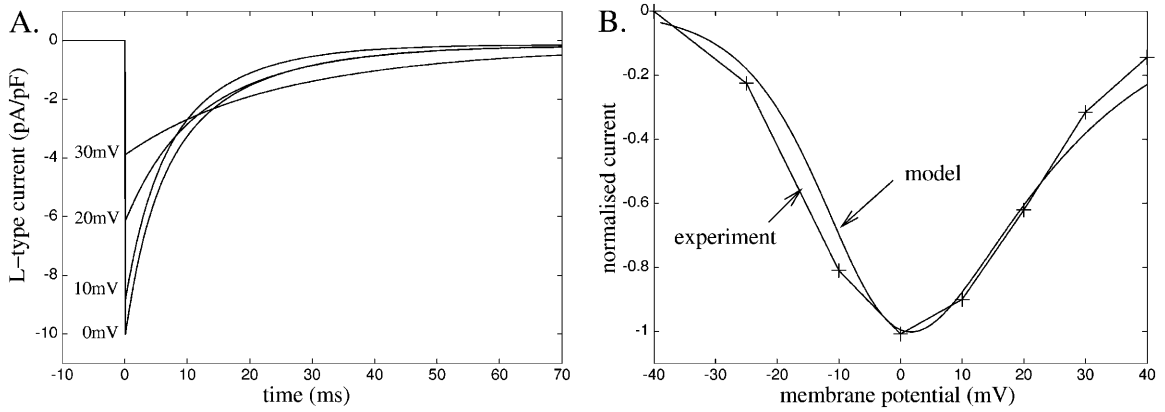

FIGURE 5 (*A*) LCC model currents generated by a step depolarization from −50 mV to a range of potentials between 0 mV and 30 mV. (*B*) The peak LCC current after a voltage step from −50 mV. The graph shows both experimental results (replotted from Fig. 1 in Zahradnikova et al., 2004) and the prediction of the model.

relationship in the model is determined by the balance among the LCC, SERCA, NCX, and sarcolemmal Ca-ATPase in a nontrivial relationship. It should be noted that intracellular $[Na^+]$ is constant in this model. The accumulation of intracellular Na^+ that occurs at high stimulation frequencies, which reduces the driving force for the NCX to remove Ca^{2+} from the cell, is another mechanism that can generate a positive force-frequency relationship.

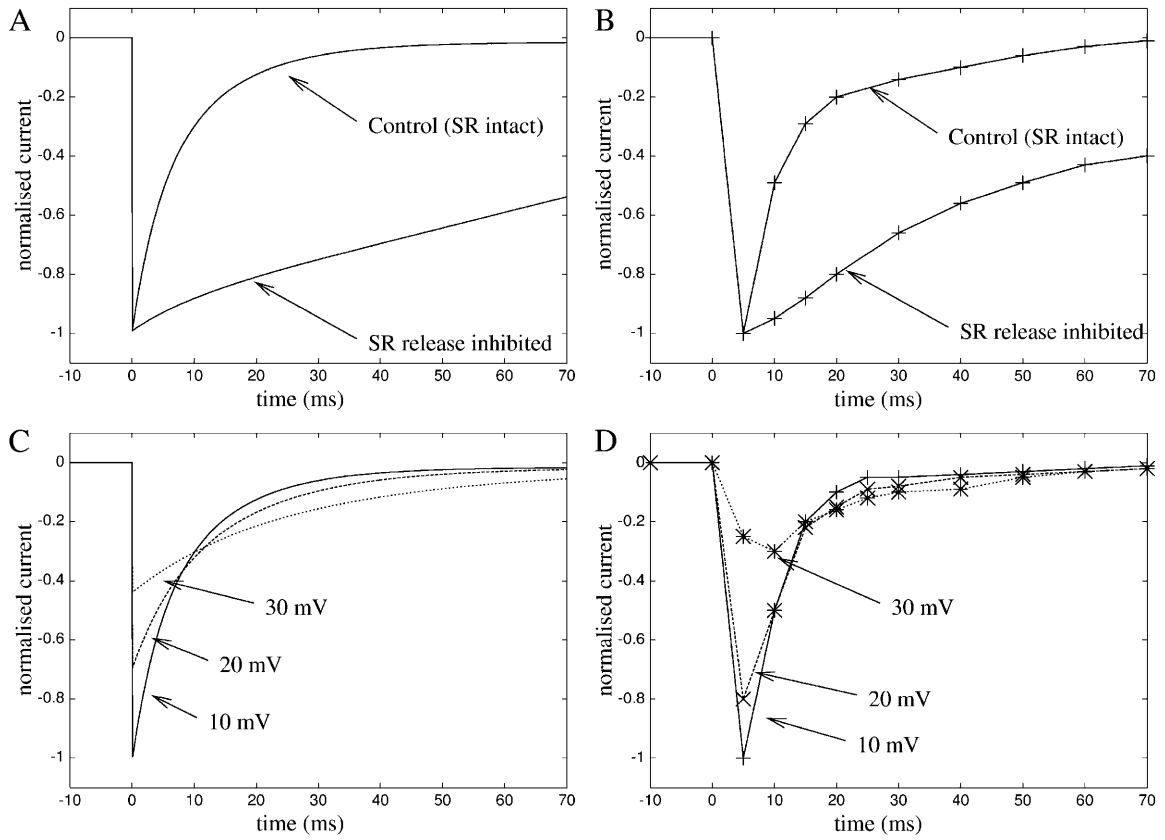

FIGURE 6 The time course of LCC current after a voltage step from −50 mV to +10 mV for the model (*A*) and from experiments (*B*) (replotted from Fig. 1 in Zahradnikova et al., 2004). Results are shown with SR Ca^{2+}-release and in the absence of SR Ca^{2+}-release. The current inactivates more slowly in the absence of SR Ca^{2+}-release, which is due to the reduction in $[Ca^{2+}]_{ds}$ and hence a reduction in the signal for Ca^{2+}-dependent inactivation of the LCCs. The time course of LCC current after a voltage step to +10 mV, +20 mV, and +30 mV, for the model (*C*) and from experiments (*D*) (replotted from Fig. 1 in Zahradnikova et al., 2004).

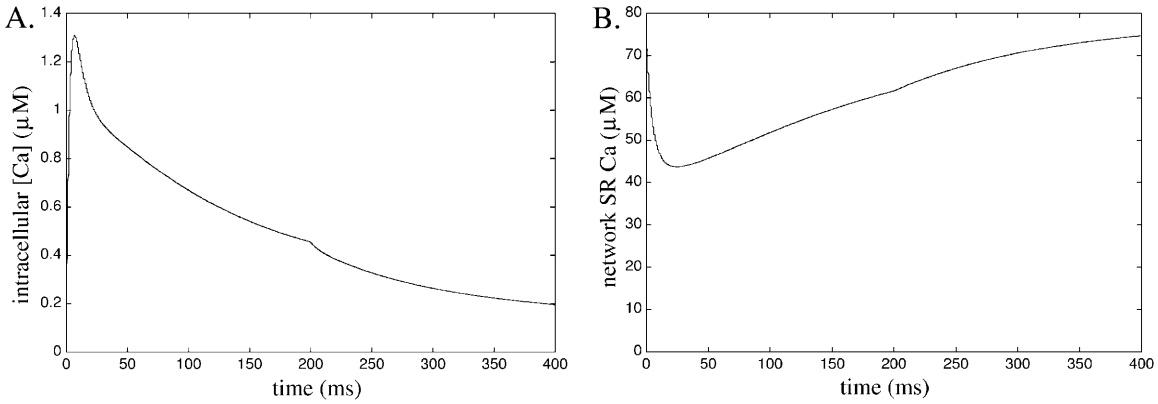

FIGURE 7 Whole-cell [Ca^{2+}] transient (*A*) and network SR Ca^{2+} load (*B*) in response to a voltage step depolarization from −80 mV to 0 mV for 200 ms with a basic cycle length of 400 ms. The SR Ca^{2+} is given in units of moles per volume of cystol. The diastolic [Ca^{2+}] is 0.2 μM and the peak [Ca^{2+}] is 1.3 μM. When the stimulation frequency is reduced to 1 Hz, the diastolic [Ca^{2+}] falls to ~0.1 μM and the peak [Ca^{2+}] falls to ~1 μM (Fig. 9).

DISCUSSION

In this article, we describe the formulation of a local control model of CICR which we refer to as the *coupled LCC-RyR gating model*. In deriving this model, we assumed that each CaRU consists of one LCC, one RyR, and the dyadic subspace within which they communicate. The CaRU model was then simplified using the following procedures. First, biophysically detailed continuous-time Markov chain models of LCC and RyR gating were simplified by identifying communicating pairs of channel states in rapid equilibrium (e.g., transitions between these states are substantially more rapid than transitions into or out of these states). These states were then coalesced, resulting in three-state models for each of these channels. Second, a rapid equilibrium approximation was used to derive an expression for $[Ca^{2+}]_{ds}$ in terms of $[Ca^{2+}]_i$ and LCC/RyR fluxes into the dyadic space, an approximation which is warranted based on the small volume of the dyadic space and the rapid efflux rate from the dyadic space. This was the critical simplifying assumption, which in turn enabled the definition of a coupled LCC-RyR gating model (Fig. 4 *A*) in which each state represents the fraction of CaRUs sharing a unique pairing of LCC and RyR states. Since the total number of unique states in the coupled LCC-RyR gating model is nine, model dynamics are described by a system of eight ordinary differential equations. Further simplifications were employed to reduce the dimensionality of this system from eight to three equations.

The advantages of this approach in modeling local control of Ca^{2+} release are the following. As in our previous model (Greenstein and Winslow, 2002), the coupled LCC-RyR gating model describes important features of local control of Ca^{2+} release, including CICR release exhibiting voltage-dependent gain. However, the approach presented here has dramatically reduced the computational cost, allowing for this model to be used readily in single cell and tissue-level simulations. The model is also based on well-accepted biophysical principles of local control of Ca^{2+} release and does not rely on more complex assumptions regarding the distribution of CaRUs containing different numbers of LCCs and RyRs (Bondarenko et al., 2004). In addition, all parameters of the coupled LCC-RyR gating model are

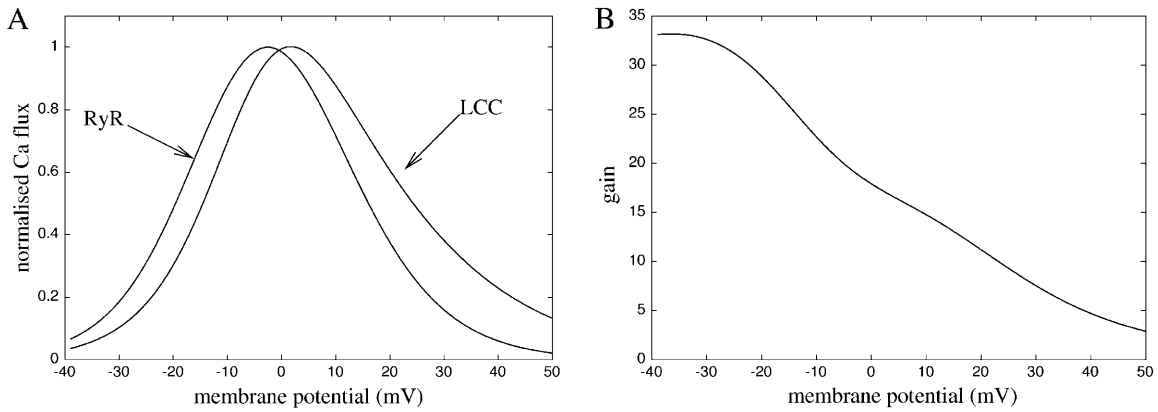

FIGURE 8 (*A*) The peak J_{LCC} and J_{RyR} as a function of membrane potential. Note that the peak of J_{LCC} lies ~10 mV to the right of J_{RyR}. (*B*) The EC-coupling gain defined by the ratio of the maximum of J_{RyR} with the maximum of J_{LCC}.

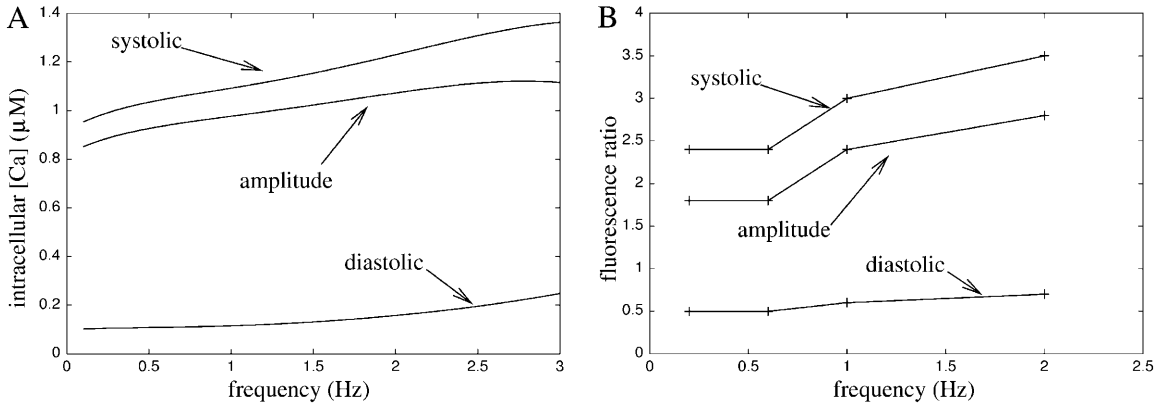

FIGURE 9 The systolic [Ca^{2+}], diastolic [Ca^{2+}], and amplitude of the Ca^{2+} transient as a function of pacing frequency for the model (*A*) and from experiments on rat ventricular trabeculae (*B*) (replotted from Fig. 2 *C* of Layland and Kentish, 1999).

derived analytically from those of the underlying LCC and RyR models. Thus, the coupled LCC-RyR model is fully constrained by the parameters defining the underlying LCC and RyR models and no additional parameters must be fit. Finally, the algorithmic procedures for model simplification (those stated above) may be implemented in software and used for the automatic generation of CaRU models based on more complex and biophysically detailed descriptions of LCC and RyR behavior. Although the resulting coupled LCC-RyR gating model will be more complex than the one described here, the channel components used to formulate these models may be defined arbitrarily. The methods described here therefore represent a general approach to the development of a family of coupled LCC-RyR gating models.

The approach described here is similar to the Ca^{2+}-synapse model presented by Stern (1992), however, the details differ in a number of important ways. First, the models of the LCC and RyR contain additional important biophysical detail, in particular the inactivation of LCCs by local Ca^{2+}, which is the predominant mechanism of LCC inactivation. Second, the rapid equilibrium approximation is derived by taking advantage of the small size of the dyadic space. This allows the effect of local [Ca^{2+}] (which depends upon the state of the LCC and RyR) on the LCC to be calculated, which is necessary to calculate the inactivation of the LCC. Third, the coupled LCC-RyR gating model was shown to reproduce experimental results which rely on local control of CICR, including inactivation of the LCC due to high [Ca^{2+}] in the dyadic space (Fig. 6), the EC gain curve (Fig. 8), fractional SR Ca^{2+} release (Fig. 7), and the force-frequency relationship (Fig. 9).

A simplifying assumption in the model was the inclusion of only one RyR in the CaRU. The main consequence of this is that release from the SR is not locally regenerative in the sense that once the single RyR closes, [Ca^{2+}] in the dyadic space decreases and no further release is generated. We are currently exploring models with multiple RyRs in the CaRU. Although these models are more efficient than Monte Carlo simulations of thousands of CaRUs, it is not possible to describe these models using a small number (<10) of coupled ordinary differential equations. As shown previously, one important feature of models with multiple RyRs in each CaRU is that they contain two metastable states and the transitions between these states occurs on timescales much longer than the individual opening of the channel (Hinch, 2004). This means that the approximation used to reduce the model from a nine-state model to a four-state model (i.e., the rate of activation of the RyRs is much faster than the rate of inactivation) would not be valid in a model containing a cluster of RyRs. Modeling work has demonstrated stochastic transitions between these metastable states could be the origin of stochastic effects observed in Ca^{2+} waves, such as the spontaneous termination of waves, the breakup of spiral waves due to noise, and array-enhanced coherence resonances (Coombes et al., 2004). However, the role, if any, of these stochastic transitions in EC coupling is unclear.

Separate local JSR volumes for each CaRU were not included in the model, which was motivated by recent experimental observations. Shannon et al. (2003) measured [Ca^{2+}] in the JSR and NSR using fluorescent indicators and found no measurable difference between the [Ca^{2+}] in the JSR and NSR during EC coupling. However, it has been noted that the timescale ($\approx$200 ms) of these measurements is much greater than the duration of a spark ($\approx$15 ms), therefore these results do not definitively rule out local depletion of the JSR as an important contributing mechanism of spark termination (Coombes et al., 2004; Stern and Cheng, 2004).

APPENDIX: MODEL EQUATIONS

The Appendix contains a summary of the model equations and estimates of the parameters from previous detailed models (Tables 1–4). The functional forms of the transition rates in the five-state LCC model are (Fig. 1 *B*)

$$\alpha_1 = e^{(V-V_L)/\Delta V_L},\ \alpha_{-1} = 1,\ k_1 = 1/t_L,$$
$$k_{-1} = \phi_L/t_L,\ \epsilon_1 = 1/K_L\tau_L \quad \text{and} \quad \epsilon_{-1} = 1/\tau_L.$$

The transition rates for the three-state model of the LCC are (Fig. 1 *C*)

$$\begin{aligned}\alpha_+ &= \frac{e^{(V-V_L)/\Delta V_L}}{t_L(e^{(V-V_L)/\Delta V_L}+1)},\\ \alpha_- &= \frac{\phi_L}{t_L},\\ \epsilon_+([Ca^{2+}]_{ds}) &= \frac{[Ca^{2+}]_{ds}(e^{(V-V_L)/\Delta V_L}+a)}{\tau_L K_L(e^{(V-V_L)/\Delta V_L}+1)},\\ \epsilon_- &= \frac{b(e^{(V-V_L)/\Delta V_L}+a)}{\tau_L(be^{(V-V_L)/\Delta V_L}+a)}.\end{aligned} \tag{12}$$

The current through the LCC is given by the Goldman-Hodgkin-Katz equation

$$J_{LCC} = J_L \delta V \frac{[Ca^{2+}]_e e^{-\delta V} - [Ca^{2+}]_{ds}}{1-e^{-\delta V}}, \tag{13}$$

where $\delta = zF/RT$. The functional forms of the transition rates in the five-state RyR model are (Fig. 2 *A*)

$$k_2 = 1/K_{RyR}^2,\ k_{-2} = 1,\ k_3 = 1/t_R,\ k_{-3} = \phi_R/t_R,$$
$$k_4 = 1/\tau_R \quad \text{and} \quad k_{-4} = \theta_R/\tau_R.$$

The transition rates for the three-state model of the RyR are (Fig. 2 *B*)

$$\begin{aligned}\beta_+([Ca^{2+}]_{ds}) &= \frac{[Ca^{2+}]_{ds}^2}{t_R([Ca^{2+}]_{ds}^2 + K_{RyR}^2)},\\ \beta_- &= \frac{\phi_R}{t_R},\\ \mu_+([Ca^{2+}]_{ds}) &= \frac{[Ca^{2+}]_{ds}^2 + cK_{RyR}^2}{\tau_R([Ca^{2+}]_{ds}^2 + K_{RyR}^2)},\\ \mu_-([Ca^{2+}]_{ds}) &= \frac{\theta_R d([Ca^{2+}]_{ds}^2 + cK_{RyR}^2)}{\tau_R(d[Ca^{2+}]_{ds}^2 + cK_{RyR}^2)}.\end{aligned} \tag{14}$$

The current through each open RyR is

$$J_{RyR} = J_R([Ca^{2+}]_{SR} - [Ca^{2+}]_{ds}). \tag{15}$$

The $[Ca^{2+}]_{ds}$ and the currents through the LCC and RyR for the different states of the CaRU are as follows.

LCC closed; RyR closed:

$$c_{CC} = [Ca^{2+}]_i. \tag{16}$$

LCC closed; RyR open:

$$\begin{aligned}c_{CO} &= \frac{[Ca^{2+}]_i + \frac{J_R}{g_D}[Ca^{2+}]_{SR}}{1+\frac{J_R}{g_D}},\\ J_{R,CO} &= J_R\frac{[Ca^{2+}]_{SR} - [Ca^{2+}]_i}{1+\frac{J_R}{g_D}}.\end{aligned} \tag{17}$$

LCC open; RyR closed:

$$\begin{aligned}c_{OC} &= \frac{[Ca^{2+}]_i + \frac{J_L}{g_D}[Ca^{2+}]_e\frac{\delta V e^{-\delta V}}{1-e^{-\delta V}}}{1+\frac{J_L}{g_D}\frac{\delta V}{1-e^{-\delta V}}},\\ J_{L,OC} &= J_L\frac{\delta V}{1-e^{-\delta V}}\frac{[Ca^{2+}]_e e^{-\delta V} - [Ca^{2+}]_i}{1+\frac{J_L}{g_D}\frac{\delta V}{1-e^{-\delta V}}}.\end{aligned} \tag{18}$$

LCC open; RyR open:

$$\begin{aligned}c_{OO} &= \frac{[Ca^{2+}]_i + \frac{J_R}{g_D}[Ca^{2+}]_{SR} + \frac{J_L}{g_D}[Ca^{2+}]_e\frac{\delta V e^{-\delta V}}{1-e^{-\delta V}}}{1+\frac{J_R}{g_D}+\frac{J_L}{g_D}\frac{\delta V}{1-e^{-\delta V}}},\\ J_{R,OO} &= J_R\frac{[Ca^{2+}]_{SR} - [Ca^{2+}]_i + \frac{J_L}{g_d}\frac{\delta V}{1-e^{-\delta V}}([Ca^{2+}]_{SR} - [Ca^{2+}]_e e^{-\delta V})}{1+\frac{J_R}{g_D}+\frac{J_L}{g_D}\frac{\delta V}{1-e^{-\delta V}}},\\ J_{L,OO} &= J_L\frac{\delta V}{1-e^{-\delta V}}\frac{[Ca^{2+}]_e e^{-\delta V} - [Ca^{2+}]_i + \frac{J_R}{g_D}([Ca^{2+}]_e e^{-\delta V} - [Ca^{2+}]_{SR})}{1+\frac{J_R}{g_D}+\frac{J_L}{g_D}\frac{\delta V}{1-e^{-\delta V}}}.\end{aligned} \tag{19}$$

The conditional probabilities of the combined states of the CaRU model (Fig. 4 *A*) are

$$
\begin{aligned}
P(y_{\mathrm{OC}}|z_1) &= \frac{\alpha_+\beta_-(\alpha_+ + \alpha_- + \beta_- + \beta_+(c_{\mathrm{CC}}))}{(\alpha_+ + \alpha_-)((\alpha_- + \beta_- + \beta_+(c_{\mathrm{OC}}))(\beta_- + \beta_+(c_{\mathrm{CC}})) + \alpha_+(\beta_- + \beta_+(c_{\mathrm{OC}})))},\\
P(y_{\mathrm{CO}}|z_1) &= \frac{\alpha_-(\beta_+(c_{\mathrm{CC}})(\alpha_- + \beta_- + \beta_+(c_{\mathrm{OC}})) + \beta_+(c_{\mathrm{OC}})\alpha_+)}{(\alpha_+ + \alpha_-)((\alpha_- + \beta_- + \beta_+(c_{\mathrm{OC}}))(\beta_- + \beta_+(c_{\mathrm{CC}})) + \alpha_+(\beta_- + \beta_+(c_{\mathrm{OC}})))},\\
P(y_{\mathrm{OO}}|z_1) &= \frac{\alpha_+(\beta_+(c_{\mathrm{OC}})(\alpha_+ + \beta_- + \beta_+(c_{\mathrm{CC}})) + \beta_+(c_{\mathrm{CC}})\alpha_-)}{(\alpha_+ + \alpha_-)((\alpha_- + \beta_- + \beta_+(c_{\mathrm{OC}}))(\beta_- + \beta_+(c_{\mathrm{CC}})) + \alpha_+(\beta_- + \beta_+(c_{\mathrm{OC}})))},\\
P(y_{\mathrm{CC}}|z_1) &= \frac{\alpha_-\beta_-(\alpha_+ + \alpha_- + \beta_- + \beta_+(c_{\mathrm{OC}}))}{(\alpha_+ + \alpha_-)((\alpha_- + \beta_- + \beta_+(c_{\mathrm{OC}}))(\beta_- + \beta_+(c_{\mathrm{CC}})) + \alpha_+(\beta_- + \beta_+(c_{\mathrm{OC}})))},
\end{aligned}
\tag{20}
$$

$$
\begin{aligned}
P(y_{\mathrm{CI}}|z_2) &= \frac{\alpha_-}{\alpha_+ + \alpha_-},\\
P(y_{\mathrm{OI}}|z_2) &= \frac{\alpha_+}{\alpha_+ + \alpha_-},\\
P(y_{\mathrm{IC}}|z_3) &= \frac{\beta_-}{\beta_+(c_{\mathrm{CC}}) + \beta_-},\\
P(y_{\mathrm{IC}}|z_3) &= \frac{\beta_+(c_{\mathrm{CC}})}{\beta_+(c_{\mathrm{CC}}) + \beta_-}.
\end{aligned}
$$

The transition rates between the combined states of the CaRU (Fig. 4 *B*) are

$$
\begin{aligned}
r_1 &= P(y_{\mathrm{OC}}|z_1)\mu_+(c_{\mathrm{OC}}) + P(y_{\mathrm{CC}}|z_1)\mu_+(c_{\mathrm{CC}}),\\
r_2 &= \frac{\alpha_+\mu_-(c_{\mathrm{OC}}) + \alpha_-\mu_-(c_{\mathrm{CC}})}{\alpha_+ + \alpha_-},\\
r_3 &= \frac{\beta_-\mu_+(c_{\mathrm{CC}})}{\beta_- + \beta_+(c_{\mathrm{CC}})},\\
r_4 &= \mu_-(c_{\mathrm{CC}}),\\
r_5 &= P(y_{\mathrm{CO}}|z_1)\epsilon_+(c_{\mathrm{CO}}) + P(y_{\mathrm{CC}}|z_1)\epsilon_+(c_{\mathrm{CC}}),\\
r_6 &= \epsilon_-,\\
r_7 &= \frac{\alpha_-\epsilon_+(c_{\mathrm{CC}})}{\alpha_+ + \alpha_-},\\
r_8 &= \epsilon_-.
\end{aligned}
\tag{21}
$$

The evolution of the subpopulations of the CaRUs are given by the law of mass action as

$$
\begin{aligned}
\frac{\mathrm{d}z_1}{\mathrm{d}t} &= -(r_1 + r_5)z_1 + r_2z_2 + r_6z_3,\\
\frac{\mathrm{d}z_2}{\mathrm{d}t} &= r_1z_1 - (r_2 + r_7)z_2 + r_8(1 - z_1 - z_2 - z_3),\\
\frac{\mathrm{d}z_3}{\mathrm{d}t} &= r_5z_1 - (r_6 + r_3)z_3 + r_4(1 - z_1 - z_2 - z_3).
\end{aligned}
\tag{22}
$$

The total whole-cell current through the LCCs and RyRs is expressed as

$$
\begin{aligned}
I_{\mathrm{RyR}} &= \frac{N}{V_{\mathrm{cyto}}}\left((J_{\mathrm{R,OO}}P(y_{\mathrm{OO}}|z_1) + J_{\mathrm{R,CO}}P(y_{\mathrm{CO}}|z_1))z_1 + \frac{J_{\mathrm{R,CO}}\beta_+(c_{\mathrm{CC}})}{\beta_- + \beta_+(c_{\mathrm{CC}})}z_3\right),\\
I_{\mathrm{LCC}} &= \frac{N}{V_{\mathrm{cyto}}}\left((J_{\mathrm{L,OO}}P(y_{\mathrm{OO}}|z_1) + J_{\mathrm{L,OC}}P(y_{\mathrm{OC}}|z_1))z_1 + \frac{J_{\mathrm{L,OC}}\alpha_+}{\alpha_- + \alpha_+}z_2\right).
\end{aligned}
\tag{23}
$$

Ca^{2+} is resequestered into the SR via the SERCA and is (Jafri et al., 1998)

$$
I_{\mathrm{SERCA}} = g_{\mathrm{SERCA}}\frac{[\mathrm{Ca}^{2+}]_{\mathrm{i}}^2}{K_{\mathrm{SERCA}}^2 + [\mathrm{Ca}^{2+}]_{\mathrm{i}}^2}.
\tag{24}
$$

The leak current from the SR to the bulk myoplasm is (Jafri et al., 1998)

$$
I_{\mathrm{SR,l}} = g_{\mathrm{SR,l}}([\mathrm{Ca}^{2+}]_{\mathrm{SR}} - [\mathrm{Ca}^{2+}]_{\mathrm{i}}).
\tag{25}
$$

The sodium-calcium exchange current is

$$
\begin{aligned}
&I_{\mathrm{NCX}}\\
&= g_{\mathrm{NCX}}\frac{e^{\eta\mathrm{VF/RT}}[\mathrm{Na}^+]_{\mathrm{i}}^3[\mathrm{Ca}^{2+}]_{\mathrm{e}} - e^{(\eta-1)\mathrm{VF/RT}}[\mathrm{Na}^+]_{\mathrm{e}}^3[\mathrm{Ca}^{2+}]_{\mathrm{i}}}{(K_{\mathrm{m,Na}}^3 + [\mathrm{Na}^+]_{\mathrm{e}}^3)(K_{\mathrm{m,Ca}} + [\mathrm{Ca}^{2+}]_{\mathrm{e}})(1 + k_{\mathrm{sat}}e^{(\eta-1)\mathrm{VF/RT}})}.
\end{aligned}
\tag{26}
$$

The sarcolemmal Ca^{2+}-ATPase is

$$
I_{\mathrm{pCa}} = \frac{g_{\mathrm{pCa}}[\mathrm{Ca}^{2+}]_{\mathrm{i}}}{[\mathrm{Ca}^{2+}]_{\mathrm{i}} + K_{\mathrm{m,pCa}}}.
\tag{27}
$$

The sarcolemmal leak current is

$$
I_{\mathrm{Cab}} = g_{\mathrm{Cab}}(E_{\mathrm{Ca}} - V),
\tag{28}
$$

where

$$
E_{\mathrm{Ca}} = \frac{RT}{2F}\ln\left(\frac{[\mathrm{Ca}^{2+}]_{\mathrm{e}}}{[\mathrm{Ca}^{2+}]_{\mathrm{i}}}\right).
\tag{29}
$$

The Ca^{2+} buffers to troponin

$$I_{\mathrm{TRPN}} = k^{-}_{\mathrm{TRPN}}([\mathrm{B}]_{\mathrm{TRPN}} - [\mathrm{TRPN}]) - k^{+}_{\mathrm{TRPN}}[\mathrm{TRPN}][\mathrm{Ca}^{2+}]_{\mathrm{i}},$$
$$\frac{\mathrm{d}[\mathrm{TRPN}]}{\mathrm{d}t} = I_{\mathrm{TRPN}}. \tag{30}$$

The rapid buffer coefficient (Wagner and Keizer, 1994) in the cytoplasm is

$$\beta_{\mathrm{i}} = \left(1 + \frac{K_{\mathrm{CMDN}}[\mathrm{B}]_{\mathrm{CMDN}}}{(K_{\mathrm{CMDN}} + [\mathrm{Ca}^{2+}]_{\mathrm{i}})^2}\right)^{-1}. \tag{31}$$

The flux balance equation for $[Ca^{2+}]_i$ and $[Ca^{2+}]_{SR}$ are

$$\frac{\mathrm{d}[\mathrm{Ca}^{2+}]_{\mathrm{i}}}{\mathrm{d}t} = \beta_{\mathrm{i}}(I_{\mathrm{LCC}} + I_{\mathrm{RyR}} - I_{\mathrm{SERCA}} + I_{\mathrm{SR,l}} - I_{\mathrm{NCX}} - I_{\mathrm{pCa}} + I_{\mathrm{Cab}} + I_{\mathrm{TRPN}}),$$
$$\frac{\mathrm{d}[\mathrm{Ca}^{2+}]_{\mathrm{SR}}}{\mathrm{d}t} = \frac{V_{\mathrm{cyto}}}{V_{\mathrm{SR}}}(-I_{\mathrm{RyR}} + I_{\mathrm{SERCA}} - I_{\mathrm{SR,l}}). \tag{32}$$

R.H. is supported by a Wellcome Trust Fellowship, and acknowledges additional travel funds (for a visit to Johns Hopkins University, where much of this work was done) from R.L.W. and Brasenose College, Oxford. This work is supported by grants from the National Institutes of Health (RO1 HL-61711, RO1 HL-60133, RO1 HL-72488, P50 HL-52307, and N01 HV-28180), The Falk Medical Trust, The Whitaker Foundation, and IBM Corporation.

REFERENCES

Alseikhan, B. A., C. D. DeMaria, H. M. Colecraft, and D. T. Yue. 2002. Engineered calmodulins reveal the unexpected eminence of Ca^{2+} channel inactivation in controlling heart excitation. *Proc. Natl. Acad. Sci. USA*. 99:17185–17190.

Bassani, J. W., W. Yuan, and D. M. Bers. 1995. Fractional SR Ca release is regulated by trigger Ca and SR Ca content in cardiac myocytes. *Am. J. Physiol. Cell Physiol.* 268:C1313–C1319.

Bers, D. M. 1993. Excitation Contraction Coupling and Cardiac Contractile Force. Kluwer Academic Press, Boston, MA.

Balke, C. W., and W. G. Wier. 1991. Ryanodine does not affect Ca^{2+} current in guinea pig ventricular myocytes in which Ca^{2+} is buffered. *Circ. Res.* 68:897–902.

Beuckelmann, D. J., and W. G. Wier. 1988. Mechanism of release of calcium from sarcoplasmic reticulum of guinea-pig cardiac cells. *J. Physiol.* (*Lond.*). 405:233–255.

Bondarenko, V. E., G. C. L. Bett, and R. L. Ramusson. 2004. A model of graded Ca^{2+} release and L-type Ca^{2+} channel inactivation in cardiac muscle. *Am. J. Physiol.* 286:H1154–H1169.

Boyett, M. R., and B. R. Jewell. 1980. Analysis of the effects of changes in rate and rhythm upon electrical activity in the heart. *Prog. Biophys. Mol. Biol.* 36:1–52.

Cannell, M. B., H. Cheng, and W. J. Lederer. 1995. The control of Ca^{2+} release in heart muscle. *Science*. 268:1045–1049.

Carmeliet, E. 2004. Intracellular Ca^{2+} concentration and rate adaptation of the cardiac action potential. *Cell Calcium*. 35:557–573.

Coombes, S., R. Hinch, and Y. Timofeeva. 2004. Receptors, sparks and waves in a fire-diffuse-fire framework for Ca^{2+} release. *Prog. Biophys. Mol. Biol.* 85:197–216.

DelBridge, L. M., J. W. Bassani, and D. M. Ber. 1996. Steady-state twitch Ca^{2+} fluxes and cytolic Ca^{2+} buffering in rabbit ventricular myocytes. *Am. J. Physiol. Cell Physiol.* 270:C192–C199.

Delgado, C., A. Artiles, A. M. Gomez, and G. Vassort. 1999. Frequency-dependent increase in cardiac Ca^{2+} current is due to reduced Ca^{2+} release by the sarcoplasmic reticulum. *J. Mol. Cell Cardiol.* 31:1783–1793.

Faber, G. M., and Y. Rudy. 2000. Action potential and contractility changes in $[Na^+]_i$ overloaded cardiac myocytes: a simulation study. *Biophys. J.* 78:2392–2404.

Frampton, J. E., C. H. Prichard, and M. R. Boyett. 1991. Diastolic systolic and sarcoplasmic reticulum $[Ca^{2+}]$ during inotropic interventions in isolated rat myocytes. *J. Physiol.* 437:351–357.

Greenstein, J. L., and R. L. Winslow. 2002. An integrative model of cardiac ventricular myocyte incorporating local control of Ca^{2+} release. *Biophys. J.* 83:2918–2945.

Handrock, R., F. Schroder, S. Hirt, A. Haverich, C. Mittmann, and S. Herzig. 1998. Single channel properties of L-type Ca^{2+} channels from failing human ventricle. *Cardiovasc. Res.* 37:445–455.

Herzig, S., P. Patil, J. Neumann, C. M. Staschen, and D. Yue. 1993. Mechanisms of β-adrenergic stimulation of cardiac Ca^{2+} channels revealed by discrete-time Markov analysis of slow gating. *Biophys. J.* 65:1599–1612.

Hinch, R. 2004. A mathematical analysis of the generation and termination of calcium sparks. *Biophys. J.* 86:1293–1307.

Hoffman, B. F., and J. J. Kelly. 1959. Effects of rate and rhythm on contraction in rat papillary muscle. *Am. J. Physiol.* 197:1199–1204.

Jafri, M. L., J. J. Rice, and R. L. Winslow. 1998. Cardiac Ca^{2+} dynamics: the roles of the ryanodine receptor adaptation and sarcoplasmic reticulum load. *Biophys. J.* 74:1149–1168.

Janczewski, A. M., H. A. Spurgeon, M. D. Stern, and E. G. Lakatta. 1995. Effects of sarcoplasmic reticulum Ca^{2+} load on the gain function of Ca^{2+} release by Ca^{2+} current in cardiac cells. *Am. J. Physiol.* 268:H916–H920.

Layland, J., and J. C. Kentish. 1999. Positive force- and $[Ca^{2+}]$ frequency relationships in rat ventricular trabeculae at physiological frequencies. *Am. J. Physiol.* 276:H9–H18.

Linz, K. W., and R. Meyer. 1998. Control of L-type ca current during the action potential of guinea-pig ventricular myocytes. *J. Physiol.* (*Lond.*). 513:425–442.

Luo, C. H., and Y. Rudy. 1994. A dynamic model of the cardiac ventricular action potential. I. Simulations of ionic currents and concentration changes. *Circ. Res.* 74:1071–1096.

Maier, L. S., D. M. Bers, and B. Pieske. 2000. Difference in Ca^{2+} handling and sarcoplasmic reticulum Ca^{2+} content in isolated rat and rabbit myocardium. *J. Mol. Cell. Cardiol.* 32:2249–2258.

Noble, D., A. Varghese, P. Kohl, and P. Noble. 1998. Improved guinea-pig ventricular cell model incorporating a dyadic space, I_{Kr} and I_{Ks}, and length- and tension-dependent processes. *Can. J. Cardiol.* 14:123–134.

Peterson, B., C. DeMaria, J. Adelman, and D. Yue. 1999. Calmodulin is the sensor for Ca^{2+}-dependent inactivation of L-type Ca^{2+} channels. *Neuron*. 22:549–558.

Peterson, B. Z., J. S. Lee, J. G. Mulle, Y. Wang, M. de Leon, and D. T. Yue. 2000. Critical determinants of Ca^{2+}-dependent inactivation within an EF-hand motif of L-type Ca^{2+} channels. *Biophys. J.* 78:1906–1920.

Pieske, B., L. S. Maier, D. M. Bers, and G. Hasenfuss. 1999. Ca^{2+} handling and sarcoplasmic reticulum Ca^{2+} content in isolated failing and nonfailing human myocardium. *Circ. Res.* 85:38–46.

Press, W. H., B. P. Flannery, S. A. Teukolosky, and W. T. Vetterling. 1989. Numerical Recipes in Pascal. Cambridge University Press, Cambridge, UK.

Rose, W. C., C. W. Balke, W. G. Wier, and E. Marban. 1992. Macroscopic and unitary properties of physiological ion flux through L-type Ca^{2+} channels in guinea-pig heart cells. *J. Physiol.* (*Lond*). 456:267–284.

Santana, L. F., H. Cheng, A. M. Gomez, M. B. Cannell, and W. J. Lederer. 1996. Relation between the sarcolemmal Ca^{2+} current and Ca^{2+} sparks and local control theories for cardiac excitation-contraction coupling. *Circ. Res.* 78:166–171.

Sham, J. S. K. 1997. Ca^{2+} release-induced inactivation of Ca^{2+} current in rat ventricular myocytes: evidence for local Ca^{2+} signalling. *J. Physiol.* 500:285–295.

Sham, J. S. K., L. S. Song, Y. Chen, L. H. Deng, M. D. Stern, E. G. Lakatta, and H. Cheng. 1998. Termination of Ca^{2+} release by a local inactivation of RyRs in cardiac myocytes. *Proc. Natl. Acad. Sci. USA.* 98:15096–15101.

Shannon, T. R., T. Guo, and D. M. Bers. 2003. Ca^{2+} scraps: local depletion of free Ca^{2+} in cardiac sarcoplasmic reticulum during contraction leave substantial Ca^{2+} in reserve. *Circ. Res.* 93:40–45.

Sipido, K., G. Callewaert, and E. Carmeliet. 1995. Inhibition and rapid recovery of Ca^{2+} during Ca^{2+} release from sarcoplasmic reticulum in guinea pig ventricular myocytes. *Circ. Res.* 76:102–109.

Sobie, E. A., K. W. Dilley, J. dos Santos Cruz, W. J. Lederer, and M. S. Jafri.2002. Termination of cardiac Ca^{2+} sparks: an investigative mathematical model of Ca^{2+}-induced Ca^{2+} release. *Biophys. J.* 83:59–78.

Sook Choi, H., and D. A. Eisner. 1999. The effects of inhibition of the sarcolemmal Ca-ATPase on systolic Ca^{2+} fluxes and intracellular Ca^{2+} concentration in rat ventricular myocytes. *Pflugers Arch.* 437:966–971.

Stern, M. D. 1992. Theory of excitation-contraction coupling in cardiac muscle. *Biophys. J.* 63:497–517.

Stern, M. D., L. S. Song, H. Cheng, J. S. K. Sham, H. T. Yang, K. R. Boheler, and E. Rios. 1999. Local control models of cardiac excitation-contraction coupling: a possible role for allosteric interactions between ryanodine receptors. *J. Gen. Physiol.* 113:469–489.

Stern, M. D., and H. Cheng. 2004. Putting out the fire: what terminates Ca^{2+}-induced Ca^{2+} release in cardiac muscle? *Cell Calcium.* 35:591–601.

Valdivia, H. H., J. H. Kaplan, G. C. R. Ellis-Davies, and W. J. Lederer. 1995. Rapid adaptation of cardiac ryanodine receptors: modulation by Mg^{2+} and phosphorylation. *Science.* 267:1997–2000.

Wagner, J., and J. Keizer. 1994. Effects of rapid buffers on Ca^{2+} diffusion and Ca^{2+} oscillations. *Biophys. J.* 67:447–456.

Wang, S. Q. L., L. S. Song, E. G. Lakatta, and H. Cheng. 2001. Ca^{2+} signalling between single L-type Ca^{2+} channels and ryanodine receptors in heart cells. *Nature.* 410:592–596.

Wier, W. G., and C. W. Balke. 1999. Ca^{2+} release mechanisms, Ca^{2+} sparks, and local control of excitation-contraction coupling in normal heart muscle. *Circ. Res.* 85:770–776.

Wier, W. G., T. M. Egan, J. R. Lopez-Lopez, and C. W. Balke. 1994. Local control of excitation-contraction coupling in rat heart cells. *J. Physiol.* 500:343–354.

Winslow, R. L., J. L. Greenstein, G. Tomaselli, and B. O'Rourke. 2001. Computational model of the failing myocyte: relating altered gene expression to cellular function. *Phil. Trans. Roy. Soc. Lond. A.* 359: 1187–1200.

Winslow, R. L., J. J. Rice, M. S. Jafri, E. Marban, and B. O'Rourke. 1999. Mechanisms of altered excitation-contraction coupling in canine tachycardia-induced heart failure. II. Model studies. *Circ. Res.* 84:571–586.

Xu, L., G. Mann, and G. Meissner. 1996. Regulation of cardiac Ca^{2+} release channel (ryanodine receptor) by Ca^{2+}, H^{+}, Mg^{2+} and adenine nucleotides under normal and simulated ischaemic conditions. *Circ. Res.* 70:1100–1109.

Zahradnik, I., and P. Palade. 1993. Multiple effects of caffeine on Ca^{2+} current in rat ventricular myocytes. *Pflugers Arch.* 424:129–136.

Zahradnikova, A., and I. Zahradnik. 1995. Description of modal gating of the cardiac Ca^{2+} release channel in planar lipid membranes. *Biophys. J.* 69:1780–1788.

Zahradnikova, A., and I. Zahradnik. 1996. A minimal gating model for the cardiac Ca^{2+} release channel. *Biophys. J.* 71:2996–3012.

Zahradnikova, A., I. Zahradnik, I. Gyorke, and S. Gyorke. 1999. Rapid activation of the cardiac ryanodine receptor by submillisecond Ca^{2+} stimuli. *J. Gen. Physiol.* 114:787–798.

Zahradnikova, A., Z. Kubalova, J. Pavelkova, S. Gyorke, and I. Zahradnik. 2004. Activation of Ca^{2+} release assed by Ca^{2+} release-induced inactivation of Ca^{2+} current in rat cardiac myocytes. *Am. J. Physiol.* 286: C330–C341.